AD-A035 927 NAVAL UNDERSEA CENTER SAN DIEGO CALIF F/G 9/2
COMPUTER-GENERATED HOLOGRAMS.(U)
DEC 76 N POS
UNCLASSIFIED NUC-TP-546 NL

| OF |
AD A035927

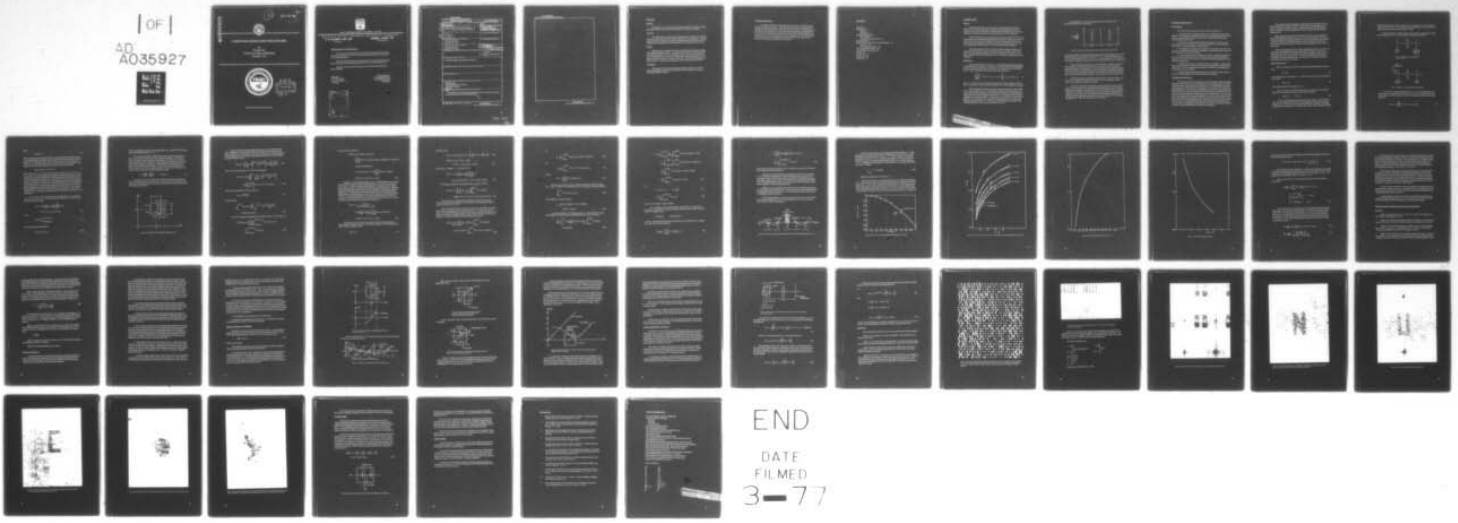

END

DATE FILMED
3-77

(12)

NUC TP 546

750

COMPUTER-GENERATED HOLOGRAMS

by
Norman Pos
Undersea Surveillance Department
December 1976

NAVAL UNDERSEA CENTER, SAN DIEGO, CA. 92132

AN ACTIVITY OF THE NAVAL MATERIAL COMMAND

R. B. GILCHRIST, CAPT, USN
Commander

HOWARD L. BLOOD, PhD
Technical Director

ADMINISTRATIVE INFORMATION

This report covers work performed at NUC in developing in-house expertise in producing synthetic binary computer-generated holograms intended for application to signal processing.

The work described herein was supported by E. P. Cooper with Independent Research funding, and took place between February 1976 and November 1976.

This report was reviewed for technical accuracy by Peter McCardell and Bruce Geelhood.

Released by
T. F. BALL, Head
System Applications
Division

Under authority of
H. A. SCHENCK, Head
Undersea Surveillance
Department

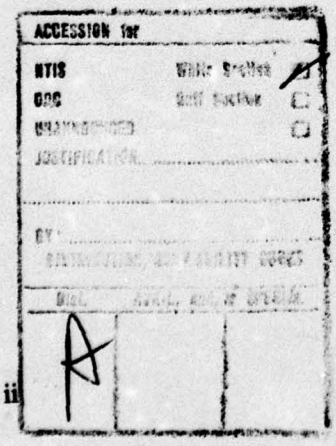

UNCLASSIFIED

SECURITY CLASSIFICATION OF THIS PAGE (When Data Entered)

REPORT DOCUMENTATION PAGE	READ INSTRUCTIONS BEFORE COMPLETING FORM
1. REPORT NUMBER: NUC TP 546	2. GOVT ACCESSION NO. / 3. RECIPIENT'S CATALOG NUMBER
4. TITLE (and Subtitle): COMPUTER-GENERATED HOLOGRAMS	5. TYPE OF REPORT & PERIOD COVERED: Research Report, Feb[illegible]–Nov[illegible]76
	6. PERFORMING ORG. REPORT NUMBER
7. AUTHOR(s): Norman Pos	8. CONTRACT OR GRANT NUMBER(s)
9. PERFORMING ORGANIZATION NAME AND ADDRESS: Naval Undersea Center, San Diego, CA 92132	10. PROGRAM ELEMENT, PROJECT, TASK AREA & WORK UNIT NUMBERS
11. CONTROLLING OFFICE NAME AND ADDRESS: Naval Undersea Center, San Diego, CA 92104	12. REPORT DATE: Dec[illegible]76 / 13. NUMBER OF PAGES: 48
14. MONITORING AGENCY NAME & ADDRESS (if different from Controlling Office)	15. SECURITY CLASS. (of this report): Unclassified / 15a. DECLASSIFICATION/DOWNGRADING SCHEDULE

16. DISTRIBUTION STATEMENT (of this Report)

Approved for public release; distribution unlimited.

17. DISTRIBUTION STATEMENT (of the abstract entered in Block 20, if different from Report)

18. SUPPLEMENTARY NOTES

19. KEY WORDS (Continue on reverse side if necessary and identify by block number)

Signal Processing
Two-Dimensional Fourier Transform
Optical Data Processing
Holograms

20. ABSTRACT (Continue on reverse side if necessary and identify by block number)

Synthetic binary computer-generated holography is used to produce the volumetric image reconstruction of real or artificial data fields.

DD FORM 1 JAN 73 1473 EDITION OF 1 NOV 65 IS OBSOLETE

UNCLASSIFIED

SECURITY CLASSIFICATION OF THIS PAGE (When Data Entered)

390 458

SUMMARY

Objective

The objective of this project was to develop the ability to produce computer-generated holograms which will provide volumetric reconstruction imaging.

Approach

The methodology for producing computer-generated holograms was studied. The state-of-the-art, as described in current publications, was investigated. Empirical studies of several techniques for producing computer-generated holograms were carried through. Theoretical and practical difficulties were identified and overcome.

Results

Synthetic binary computer-generated holograms have been used to produce real imaging of volumetric objects. A hologram of the image of an arbitrary object can now be produced on demand. Requisite computer time per object plane for a 64 X 64 data field has been reduced by refinements in programming from over 10 minutes to about 1 minute of central processor time. The cost of producing a hologram, exclusive of plotting and photography, has been reduced to about $7.00.

Conclusions

The process of real-time two-dimensional signal processing via computer-generated holograms is within reach, and awaits only the emergence of practical spatial light modulator devices.

ACKNOWLEDGMENTS

The author would like to express his appreciation to the following people for their most gracious assistance: Neal Martini for his guidance and support; Pete McCardell for his optics expertise; Bruce Geelhood for our many fruitful theoretical discussions; Larry Sammons who, with patience and compassion, photographically reduced the many hologram plots and also produced the photographic plates in this report; the crew in the 1110 operating room who tended the Cal Comp Plotter with fortitude during the many hologram plots made during this work; and Dr. E. P. Cooper for his generous sponsorship of this problem.

CONTENTS

INTRODUCTION

General

The appearance of the now classic paper by Lohmann and Paris (Ref. 1) ushered in an era of synthetic binary computer-generated holograms at various research centers. NUC is interested in these synthetic holograms for their potential application to real-time optical processing of underwater acoustic signal data.

This report shall describe the progress which has been made at NUC in developing expertise in computer-generated holograms intended for signal processing. The scope of the work covers the methodology of synthetic hologram production, the development and refinement of computer programs for hologram production, and the demonstration in the laboratory of the functioning of these holograms.

The report shall derive the fundamental synthetic hologram equation, criticize it, develop alternative methods of hologram production, discuss "tricks of the trade" for improving image quality, extend the development from planar to volumetric imaging, and finally recommend future work necessary to refine this in-house capability.

Background

The Convolution Theorem states that convolving two functions is equivalent to multiplying their transforms. If we employ the usual convention of allowing capital letters to represent the Fourier transforms of their respective lower-case letters, then to within a normalization constant, the theorem states that

$$F\left[\iint_{-\infty}^{\infty} g(\xi, \eta)\, h(x-\xi, y-\eta)\, d\xi\, d\eta\right] = G(\nu_x, \nu_y)\, H(\nu_x, \nu_y) \qquad (1)$$

where F will be used to denote the Fourier transform. We have written the relationship in two variables because we shall be working in this mode throughout this report.

That the transfer function of an ordinary convex lens exhibits a form similar to Eq. 1 has long been known. This observation naturally leads to conceiving of an optical system capable of taking a two-dimensional transform and performing convolution and hence correlation (where h and H in Eq. 1 are replaced by their complex conjugates) "at the speed of light." This concept, in turn, leads to the attractive possibility of a vast reduction in the computation times required by the various tasks involved in signal processing – *if*, that is, the optical transparencies needed for the computational task at hand can be produced in "real time."

As an example, Fig. 1 shows an optical setup for performing a two-dimensional correlation or convolution:

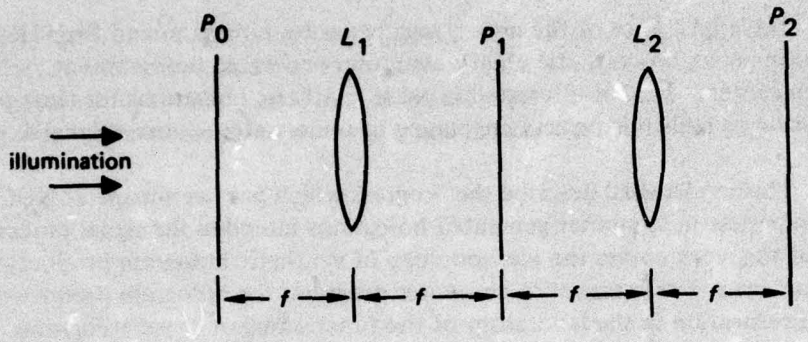

Figure 1. Optical setup for performing a two-dimensional correlation or convolution.

P_0 is the input plane, with transmittance proportional to the input data $g(x, y)$. The Fourier transform of F_0 appears at plane P_1 as $G(\nu_x, \nu_y)$. If the transmittance of plane P_1 is proportional to $H(\nu_x, \nu_y)$ or $H^*(\nu_x, \nu_y)$, then the plane P_2 will contain the convolution or correlation, respectively, of the two input functions $g(x, y)$ and $h(x, y)$.

Now, the transmittances of P_0 or P_1 or both should be capable of being controlled at will in order for this optical device to function in a real-world signal-processing situation. For example, since P_1 is a transform plane, pre-prepared holographic data might be inserted there as a fixed transmittance, and plane P_0 might be one of the several "spatial light modulator" devices which at this writing are promising to emerge from the domain of research to become practical devices (Ref. 2–6).

Should the apparatus schematically shown in Fig. 1 become a reality, a vast improvement in signal-processing rates could be achieved, particularly with the advent of volumetric reconstruction capability.

The promise which optical signal processing thus holds out, that of the correlation and convolution of two signal parameters simultaneously and sufficiently rapidly to allow signal processing in real time, requires the production of synthetic holograms "on demand." The entire process can conveniently be divided into that research effort directed toward the refinement of spatial light modulator devices and that directed toward the development of computer techniques for producing holographic data. This report addresses itself to the latter.

SYNTHETIC HOLOGRAMS

Characteristics

Among the attractive characteristics of synthetic holograms are –

1. The image need not physically exist. Only a mathematical description is required. Thus, holograms of signal characteristics of oceanographic targets of interest may be prepared in the absence of "hard" data. Theoretical models of ship acoustic signatures will suffice.

2. In contrast to the traditional "physical" production of holograms, the object volume is not constrained in any way by illumination coherence, vibration, air turbulence during photography, or similar effects.

3. The production of optical code translators, inverse filters, and other such complex computational transparencies (holograms) is considerably easier when done by computer than when done physically.

4. Unlike physically produced holograms, whose "modulation parameter" is fixed by the ratio of intensities of the reference and object waves, the synthetic hologram can easily be produced with an optimized modulation parameter by clever computer programming.

5. The binary nature of the hologram itself is an advantage: A binary hologram (in contrast to the usual gray-scale holograms) is insensitive to nonlinear photographic films. Thus, the transmission–exposure characteristic of the photographic emulsion is not now a constraint.

6. Binary computer-generated holograms can be made to be more efficient in terms of image brightness than physically produced holograms.

Fundamentals of Production

The basic idea used in the production of binary synthetic computer-generated holograms is to produce an array of diffracting holes (transparent areas) in an otherwise opaque film. Each such hole must somehow carry in its descriptive parameters information which will control both the amplitude and the phase of the transmitted (diffracted) light. To this end, the usual approach is to specify that the hologram be illuminated in such a way that the phase of the illumination at the plane of the hologram be a known function of the coordinates of the hologram plane. Then the holes may determine the phase of the diffracted light by their relative position in the phase-plane. The amplitude of the diffracted light may be controlled most simply by varying the size of the holes, although there are other means for achieving this, as will be described later. It is instinctively preferable to describe the hole so that the variations in its size are orthogonal to the variations in its position in order that potential "mixing" of phase and amplitude information be minimized.

For example, should the hologram be illuminated by a near-field source so that the illumination is spherical, then one would realize a phase-sensitivity of the holes by varying their positions radially. Amplitude control would then suggest itself as a variation in hole size tangentially to a set of concentric circles upon the hologram plane.

Many other such schemes can obviously be contrived, and it is conceivable that special applications may require any one of them. In this paper we shall concentrate on perhaps the simplest arrangement (and the most popular in the scientific community), wherein the illumination falls upon the hologram as a tilted planar wave front, thus producing a phase variation across the hologram plane in one coordinate only.

Much of the following work is a direct embellishment of Ref. 1, but the "fit" is not exact. We shall depart from that classic paper as necessary. Some of the departures will be radical. Nevertheless, the referenced paper may be said to be a prerequisite for what is to be said here. The work to immediately follow will be restricted to the topic of planar objects. The extension to volumetric reconstruction will be covered later in this report.

BASIC DERIVATION

By way of defining our terms, we may start by specifying a square object of sides

$$\Delta x = \Delta y \tag{2}$$

in the object plane of coordinates (x, y). In like manner, we specify the square hologram of sides

$$\Delta \nu_x = \Delta \nu_y \tag{3}$$

in the transform plane of coordinates (ν_x, ν_y).

We next conceive of resolution elements $\delta\nu$, δx in the transform plane and object plane, respectively, and connect them with the relations

$$\Delta x \delta \nu = 1; \qquad \delta x \Delta \nu = 1 \tag{4}$$

It is not necessary that these products be unity. That is, one may choose to have arrays of resolution elements upon the hologram and upon the object plane unequal in size. The choice of unity is simply an analytic convenience. Note that coordinates ν have dimensions of 1/length. They are the "space frequency variables"

(cycles/centimeter, if you will). *Length* units to be measured upon the hologram are found from $\lambda f\nu$, where λ is the wavelength of the light employed, and f is the focal length of the lens (all in compatible units of course).

Now, the process to be synthesized on the computer is diagrammed in Fig. 2, and the application of the resulting hologram is diagrammed in Fig. 3:

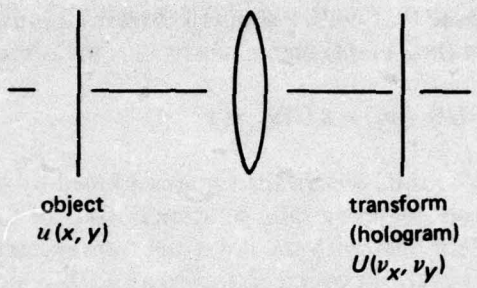

Figure 2. Optical process to be synthesized on the computer.

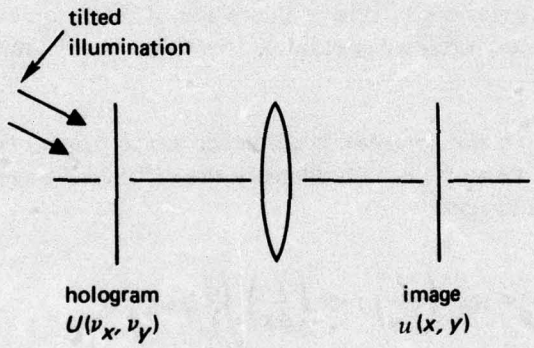

Figure 3. Application of the synthetically produced hologram.

If we desire a (complex) image function $u(x, y)$ in the image plane to be a consequence of a transform plane function $U(\nu_x, \nu_y)$, we can by dint of the transform properties of the lens relate U and u by the familiar two-dimensioned Fourier transform:

$$U(\nu_x, \nu_y) = \iint u(x, y)\, E(-x\nu_x - y\nu_y)\, dxdy \qquad (5)$$

where

$$E(x) \equiv e^{2\pi i x} \tag{6}$$

will be a convenient functional abbreviation. If we illuminate the transform plane by a collumated plane wave tilted in the x direction only, the phase in the transform plane of the incident illumination will not be a function of y, and thus takes the form $E(x_0 \nu_x)$. We propose that, with a properly contrived binary amplitude transmission in the transform (hologram) plane, where x_0 is the source offset:

$$E(x_0 \nu_x)\, H(\nu_x, \nu_y) = KU(\nu_x, \nu_y) \tag{7}$$

We will require Eq. 7 to be valid within the squares defined by $|\nu_{x,y}| \leqslant \Delta y/2$ and $|x|,|y| \leqslant \Delta x/2$. We will not require a valid solution outside of these squares. That is, the product of the incident light with the hologram transmittance must be proportional to the diffracted wavefront over a restricted area. K is a constant of proportionality which will from time to time absorb unimportant numerical multiplicative factors, as we shall see. The reason for restricting the solution to only a part (albeit the significant part) of the plane is that otherwise the system will not be solvable. Binary holograms are, after all, approximations to the "real thing." By "releasing" all constraints on the solution outside of the region of interest we will gain some analytic leverage. At any rate, we are always free to mask off unwanted parts of the image plane.

Now if $h(x,y)$ is the complex signal in the image plane $u(x,y)$ diffracted from $H(\nu_x, \nu_y)$, then we may formally identify the diffracted wavefront as proportional to the required image:

$$h(x,y) = \text{rect}\left(\frac{x}{\Delta x}\right) \text{rect}\left(\frac{y}{\Delta x}\right) \iint H(\nu_x, \nu_y) \cdot E\left[(x + x_0)\,\nu_x + y\nu_y\right] d\nu_x\, d\nu_y \tag{8}$$

where

$$\text{rect}(x) \equiv \begin{cases} 1 \text{ if } |x| \leqslant 1/2 \\ 0 \text{ otherwise} \end{cases} \tag{9}$$

and we specify the identification:

$$h(x,y) = Ku(x,y) \tag{10}$$

That is, the diffracted wavefront at the image plane, $h(x,y)$, must be at least proportional to the required pattern, $u(x,y)$.

The entire process will be a discrete rather than a continuous procedure, since we have a digital computer to pass the equations through. To this end we invent a rectangular mesh of points in the hologram plane, indexed by n in the x direction and by m in the y direction. To each point of this discrete mesh we seek to calculate and assign two parameters, corresponding to the amplitude and the phase of the transmittance at that point. The area of the object divided by the object resolution is the number of discrete points N^2 resolvable in the image, and because of Eq. 4, also to be calculated upon the hologram:

$$N^2 = \frac{\Delta x \Delta y}{\delta x \delta y} = \left(\frac{\Delta x}{\delta x}\right)^2; \qquad N = \Delta x \Delta \nu \tag{11}$$

At each point we erect a square $\delta\nu$ on a side, this being our resolution cell (Fig. 4). Within each cell we produce a hole. The area of the hole will control the amplitude, and the displacement of the hole in the x direction will control the phase of the diffracted wavefront:

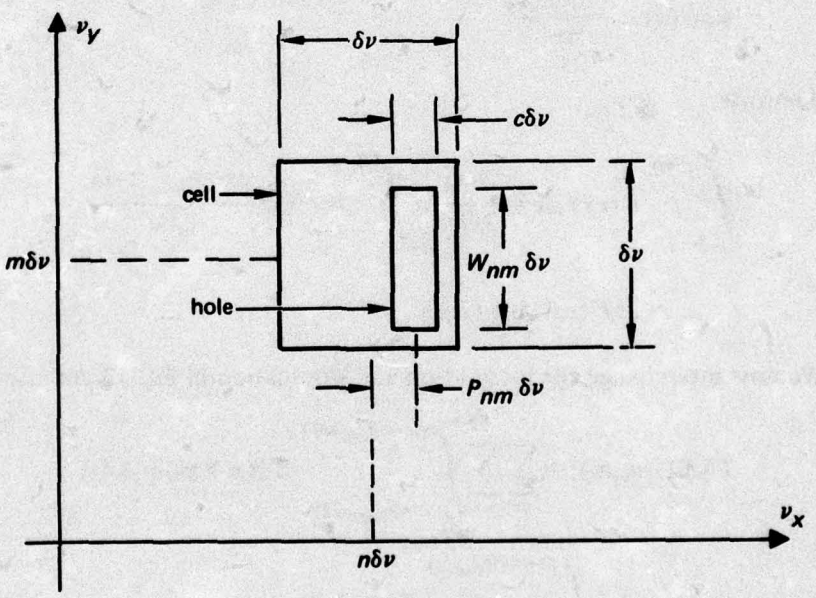

Figure 4. Detailed sketch of the resolution cell containing its hole.

Note that in the y direction the hole position is a constant while the hole size is a variable, and just the reverse holds in the x direction. Our plan now is to take a specified $u(x,y)$ and produce a set of W_{nm} and P_{nm} for use in constructing the holes according to Fig. 4. The binary transmission function of the entire hologram can then be directly written:

$$H(\nu_x,\nu_y) = \sum_n \sum_m \text{rect}\left[\frac{\nu_x - (n + P_{nm})\,\delta\nu}{c\delta\nu}\right] \text{rect}\left(\frac{\nu_y - m\delta\nu}{W_{nm}\,\delta\nu}\right) \tag{12}$$

Now we reverse-transform Eq. 7 to obtain the image plane:

$$F(KU) = F(EH) = \iint_{-\infty}^{\infty} \sum_n \sum_m \text{rect}\left[\frac{\nu_x - (n + P_{nm})\,\delta\nu}{c\delta\nu}\right]$$

$$\cdot\ \text{rect}\left[\frac{\nu_y - m\delta\nu}{W_{nm}\,\delta\nu}\right] E\left[(x + x_0)\,\nu_x + y\nu_y\right]\, d\nu_x\, d\nu_y \tag{13}$$

We will need the definition of the sinc function

$$\text{sinc}\,(x) \equiv \frac{\sin(\pi x)}{\pi x} \tag{14}$$

and the identity

$$\int_{a-b}^{a+b} E(cx)\,dx = \frac{\epsilon^{2\pi icx}}{2\pi ic}\Bigg|_{a-b}^{a+b} = \epsilon^{2\pi ica}\,\frac{\epsilon^{2\pi icb} - \epsilon^{-2\pi icb}}{2\pi ic}$$

$$= 2bE(ca)\,\text{sinc}\,(2cb) \tag{15}$$

We now interchange the integration and summation in Eq. 13 and use Eq. 11:

$$F[KU(\nu_x,\nu_y)] = \sum_n \sum_m \int_{\delta\nu(n+P_{nm}-c/2)}^{\delta\nu(n+P_{nm}+c/2)} E\left[(x + x_0)\,\nu_x\right] d\nu_x$$

$$\cdot \int_{\delta\nu(m-W_{nm}/2)}^{\delta\nu(m+W_{nm}/2)} E(y\nu_y)\,d\nu_y \tag{16}$$

And now use Eq. 10 and 15:

$$F[KU(\nu_x, \nu_y)] = Ku(x,y) = h(x,y)$$

$$= \sum_n \sum_m c\delta\nu E\,[(x + x_0)\,\delta\nu\,(n + P_{nm})]\ \text{sinc}\,[c\delta\nu\,(x + x_0)]\,W_{nm}\,\delta\nu$$

$$\cdot\, E\,(ym\delta\nu)\ \text{sinc}\,(yW_{nm}\,\delta\nu)$$

$$= c\,(\delta\nu)^2\ \text{sinc}\,[c\delta\nu\,(x + x_0)] \sum_n \sum_m W_{nm}\ \text{sinc}\,(yW_{nm}\,\delta\nu)$$

$$\cdot\, E\left\{\delta\nu\,[(x + x_0)\,(n + P_{nm}) + ym]\right\} \qquad (17)$$

Equation 17 is a detailed description of $h(x,y)$. Unfortunately it is not a pure Fourier series or it could be solved by equating it term for term to the series expansion of $u(x,y)$, to within a proportionality constant. The departures from a pure Fourier series are three: the two sinc functions and part of the exponent. Physically, these terms can be said to have arisen from the approximate nature of the synthetic hologram. It is true that they may be ignored, but at the expense of degrading the image quality. In the following work, a way will be found to an asymptotic solution of Eq. 17. To start, the leading sinc term outside the summation may be directly computed, then divided into the $u(x,y)$ array to produce a new array, $v(x,y)$. At the same time, we may absorb the constant term $c(\delta\nu)^2$ into K.

$$Kv(x,y) = \frac{Ku(x,y)}{c\,(\delta\nu)^2\ \text{sinc}\,[c\delta\nu\,(x + x_0)]}$$

$$= \text{rect}\left(\frac{x}{\Delta x}\right) \text{rect}\left(\frac{y}{\Delta x}\right) \sum_n \sum_m W_{nm}\ \text{sinc}\,(yW_{nm}\,\delta\nu)$$

$$\cdot\, E\left\{\delta\nu\,[(x + x_0)\,(n + P_{nm}) + ym]\right\} \qquad (18)$$

We have also at this time taken the liberty to restrict the solution to the square image, as discussed previously. The following analysis will be simplified if the source offset x_0 is chosen so that

$$x_0\,\delta\nu = M \qquad (19)$$

an integer. Then

$$c\delta\nu\,(x + x_0) = c\delta\nu\,(n\delta x + x_0) = c\left(n\,\frac{\delta x}{\Delta x} + \delta\nu x_0\right) = c\left(\frac{n}{N} + M\right) \tag{20}$$

$$E\left\{\delta\nu\,[(x + x_0)\,(n + P_{nm}) + ym]\right\}$$

$$= E\,[x\delta\nu\,(n + P_{nm}) + MP_{nm} + ym\delta\nu] \tag{21}$$

since $E\,(Mn) = E\,(\text{integer}) = 1$. Then from Eq. 18:

$$Kv\,(x,y) = \text{rect}\left(\frac{x}{\Delta x}\right)\text{rect}\left(\frac{y}{\Delta x}\right)\sum_n\sum_m W_{nm}$$

$$\cdot\,\text{sinc}\,(yW_{nm}\,\delta\nu)\,E\,[xn\delta\nu + ym\delta\nu + xP_{nm}\,\delta\nu + MP_{nm}] \tag{22}$$

Now take the transform of both sides of Eq. 22, where $V = F(\nu)$:

$$KV\,(\nu_x, \nu_y) = \sum_n\sum_m W_{nm}\,\frac{1}{(\Delta x)^2}\iint_{-\Delta x/2}^{\Delta x/2}\text{sinc}\,(yW_{nm}\,\delta\nu)$$

$$\cdot\,E\,[MP_{nm} + (n - j)\,x\delta\nu + (m - k)\,y\delta\nu + xP_{nm}\,\delta\nu]\,dxdy \tag{23}$$

The rect functions went over to the integration limits, and the sampled Fourier transform was accomplished in the usual way by multiplying the exponential in Eq. 22 by $E\,[(-jx - ky)\,\delta\nu]$.

Now (j,k), which show in Eq. 23 for the first time, are the indices of a square matrix which is a mapping of the (n,m) matrix of Eq. 22. We intend to construct this (j,k) matrix from the given (n,m) data, from which V is numerically derived, and relate it to the matrix of amplitudes W and angles P, which will allow the holes to be produced. To this end, we proceed with the integrations in Eq. 23:

$$KV_{jk} = \frac{1}{(\Delta x)^2}\sum_n\sum_m W_{nm}\,E\,(MP_{nm})\int_{-\Delta x/2}^{\Delta x/2}\text{sinc}\,(yW_{nm}\,\delta\nu)$$

$$\cdot\,E\,[(m - k)\,y\delta\nu]\,dy\int_{-\Delta x/2}^{\Delta x/2}E\,[(n - j)\,x\delta\nu + xP_{nm}\,\delta\nu]\,dx \tag{24}$$

Let

$$\sigma_y = \frac{1}{\Delta x} \int_{-\Delta x/2}^{\Delta x/2} \text{sinc}\,(y W_{nm}\,\delta\nu)\, E\,[(m-k)\, y\delta\nu]\, dy \tag{25}$$

Let

$$\sigma_x = \frac{1}{\Delta x} \int_{-\Delta x/2}^{\Delta x/2} E\left\{x\,[(n-j)\,\delta\nu + P_{nm}\,\delta\nu]\right\} dx \tag{26}$$

So that

$$KV_{jk} = \sum_n \sum_m W_{nm}\, E\,(MP_{nm})\, \sigma_y\, \sigma_x \tag{27}$$

We may now attempt to render the sigmas amenable to machine computation: In Eq. 15, setting $a = 0$ and putting b over to $b/2$ results in the related identity:

$$\int_{-b/2}^{b/2} E\,(cx)\, dx \equiv b\ \text{sinc}\,(cb) \tag{28}$$

from which Eq. 26 can be described:

$$\sigma_x = \frac{1}{\Delta x}\,\Delta x\ \text{sinc}\left\{\Delta x\,[(n-j)\,\delta\nu + P_{nm}\,\delta\nu]\right\}$$

$$= \text{sinc}\,(n - j + P_{nm}) \tag{29}$$

σ_y is more complicated: We introduce into Eq. 25 the well-known Fourier representation of the sinc function (and temporarily drop the W subscripts):

$$\frac{1}{W\delta\nu} \int_{-\infty}^{\infty} \text{rect}\left(\frac{u}{W\delta\nu}\right) E\,(uy)\, du = \frac{1}{W\delta\nu} \int_{-W\delta\nu/2}^{W\delta\nu/2} E\,(uy)\, du$$

$$= \text{sinc}\,(yW\delta\nu) \tag{30}$$

$$\sigma_y = \frac{1}{\Delta x} \int_{y=-\Delta x/2}^{\Delta x/2} \frac{1}{W\delta\nu} \int_{u=-W\delta\nu/2}^{W\delta\nu/2} E(uy)\, du\, E[y\delta\nu(m-k)]\, dy$$

$$= \frac{1}{W} \int_{u=-W\delta\nu/2}^{W\delta\nu/2} \int_{y=-\Delta x/2}^{\Delta x/2} E\left\{y\,[u+\delta\nu\,(m-k)]\right\} dy\, du$$

$$= \frac{1}{W} \int_{-W\delta\nu/2}^{W\delta\nu/2} \Delta x\ \mathrm{sinc}\left\{\Delta x\,[u+\delta\nu\,(m-k)]\right\} du$$

$$= \frac{\Delta x}{W} \int_{-W\delta\nu/2}^{W\delta\nu/2} \mathrm{sinc}\,(\Delta x u + m - k)\, du \tag{31}$$

Let

$$w = \Delta x u + m - k; \qquad du = \frac{dw}{\Delta x} \tag{32}$$

$$\sigma_y = \frac{1}{W} \int_{m-k-W/2}^{m-k+W/2} \mathrm{sinc}\, w\, dw \tag{33}$$

where w now is simply a dummy variable.

Let us now gather this material together and rewrite Eq. 27 using what we now know. In addition, let us go over to phasor notation, letting P and Q be decimal parts of 2π radians, so that:

$$|P|, |Q| \leqslant \frac{1}{2}; \qquad |2\pi P|, |2\pi Q| \leqslant \pi$$

And let us express the complex matrix element KV_{jk} as an amplitude A_{jk} at an angle Q_{jk}. Then Eq. 27 assumes the form:

$$A_{jk} \angle Q_{jk} = \sum_n \sum_m W_{nm} \angle MP_{nm}\, \sigma_x \sigma_y \tag{34}$$

$$= \sum_n \sum_m W_{nm} \angle MP_{nm} \operatorname{sinc}(n - j + P_{nm})$$

$$\cdot \frac{1}{W_{nm}} \int_{m-k-W_{nm}/2}^{m-k+W_{nm}/2} \operatorname{sinc} w \, dw \tag{34}$$

where the two Ws are not canceled, because we will want to keep the $1/W$ attached to the integral for the following work.

Equation 34 is our prescription for mapping the elements of the complex $N \times N$ (j,k) matrix (considered as computed from the given $u(x,y)$) to the $N \times N$ (n,m) matrix, which is to be found. Again, note that one could approximate the two sigmas to unity when $n = j$ and $m = k$, respectively, and put them to zero otherwise. The resulting identification of A_{jk} directly to W_{jk} and likewise of Q_{jk} to MP_{jk} would constitute a zeroth-order approximation.

Whether or not one does that, the physical role of the parameter M is clear: The larger M gets, the less the deviation of each hole from cell center, and the steeper the illumination angle is required to be. The primary image formed will also move out to higher orders as M increases.

The remaining integral σ_y cannot be expressed in closed form. We may find a suitable approximation to it by the following observations: First, let us study Fig. 5, which is a plot of the integral σ_y.

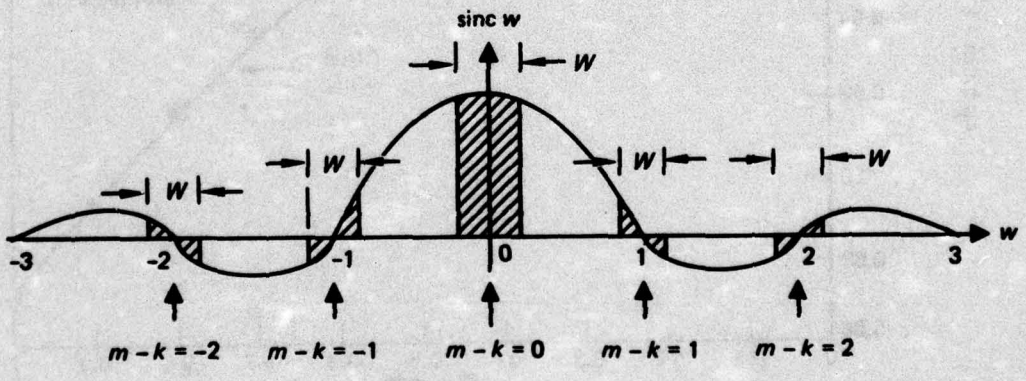

Figure 5. Plot of Eq. 33. The shaded areas represent the values of the integral for various values of $m - k$.

The shaded areas in Fig. 5 are the integrals for various values of $m - k$. Considering the $1/W$ in front of the integral, it is heuristically clear that the $m = k$ term dominates and is approximately +1. For $m - k = \pm 1$ we can expect σ_y to be small and positive; for $m - k = \pm 2$, σ_y is smaller yet and negative, and so on. We may now represent σ_y with two alternative approximations, one for $m = k$ and the other for $m \neq k$. A straightforward application of a least-squares fit of a quadratic polynomial to σ_y for $m = k$ yields:

$$\sigma_y \Big|_{m=k} = 1 - 0.129\, W_{nk}^2 \tag{35}$$

Figure 6 is a plot of σ_y for the case $m = k$.

As for the case when $m \neq k$, numerical plots for σ_y for various combinations of $m - k$ and W were studied. It was discovered that plots of σ_y against W for various values of $(m - k)$ very nearly paralleled each other (see Fig. 7). This suggests that σ_y can be broken into two convenient factors, one a function of W alone, which could then be normalized, and the other a function of $m - k$ alone, which could be called a "denormalizing" function, if you will. These are plotted in Fig. 8 and 9, respectively.

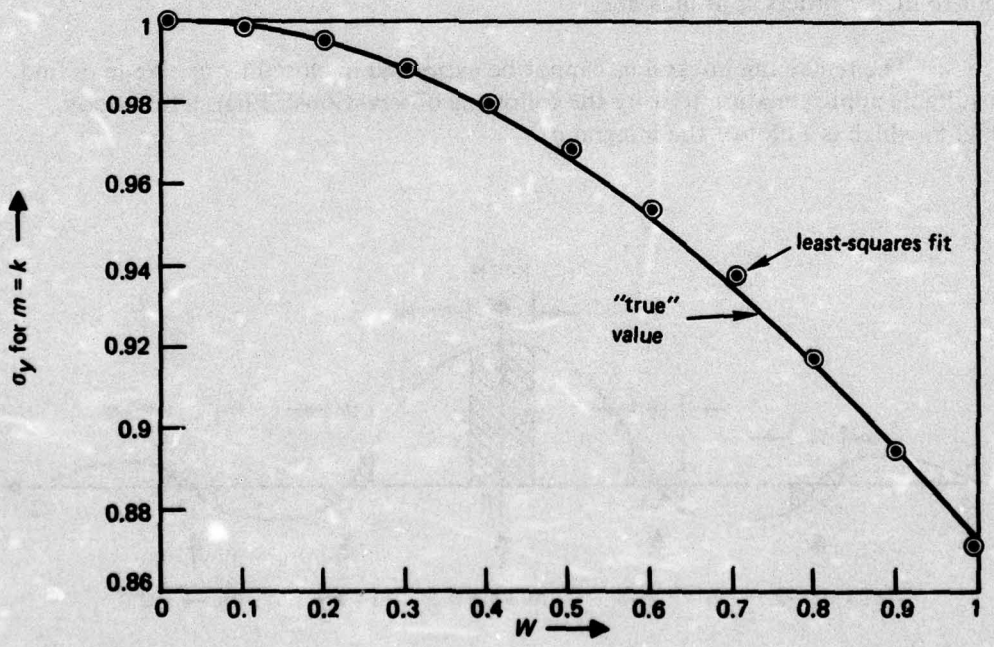

Figure 6. Plot of Eq. 33 for $m = k$, indicating the least-squares fit to the data.

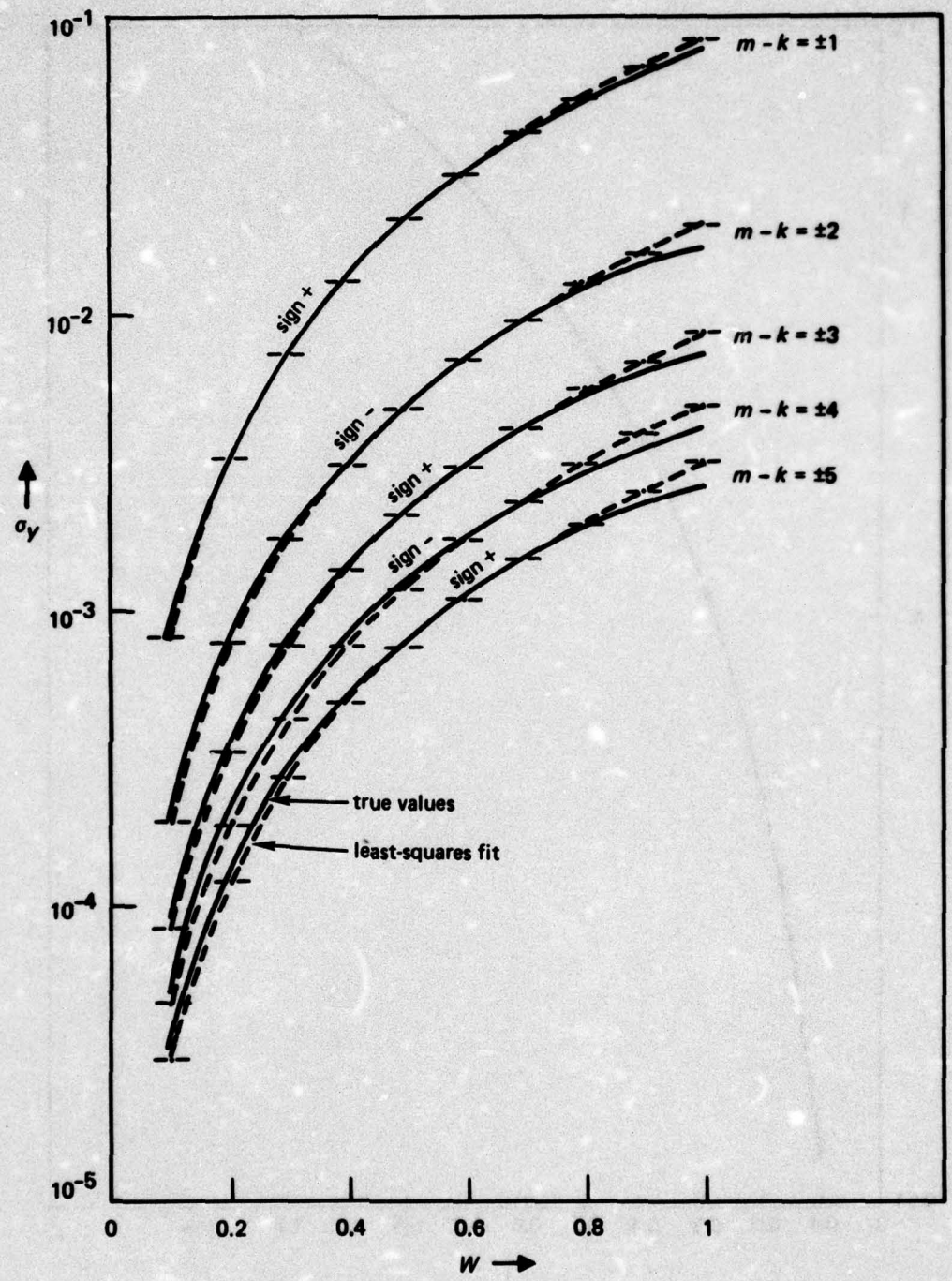

Figure 7. Plot of Eq. 33 when $m \neq k$, with $m - k$ as a parameter, indicating the least-squares fit to the data.

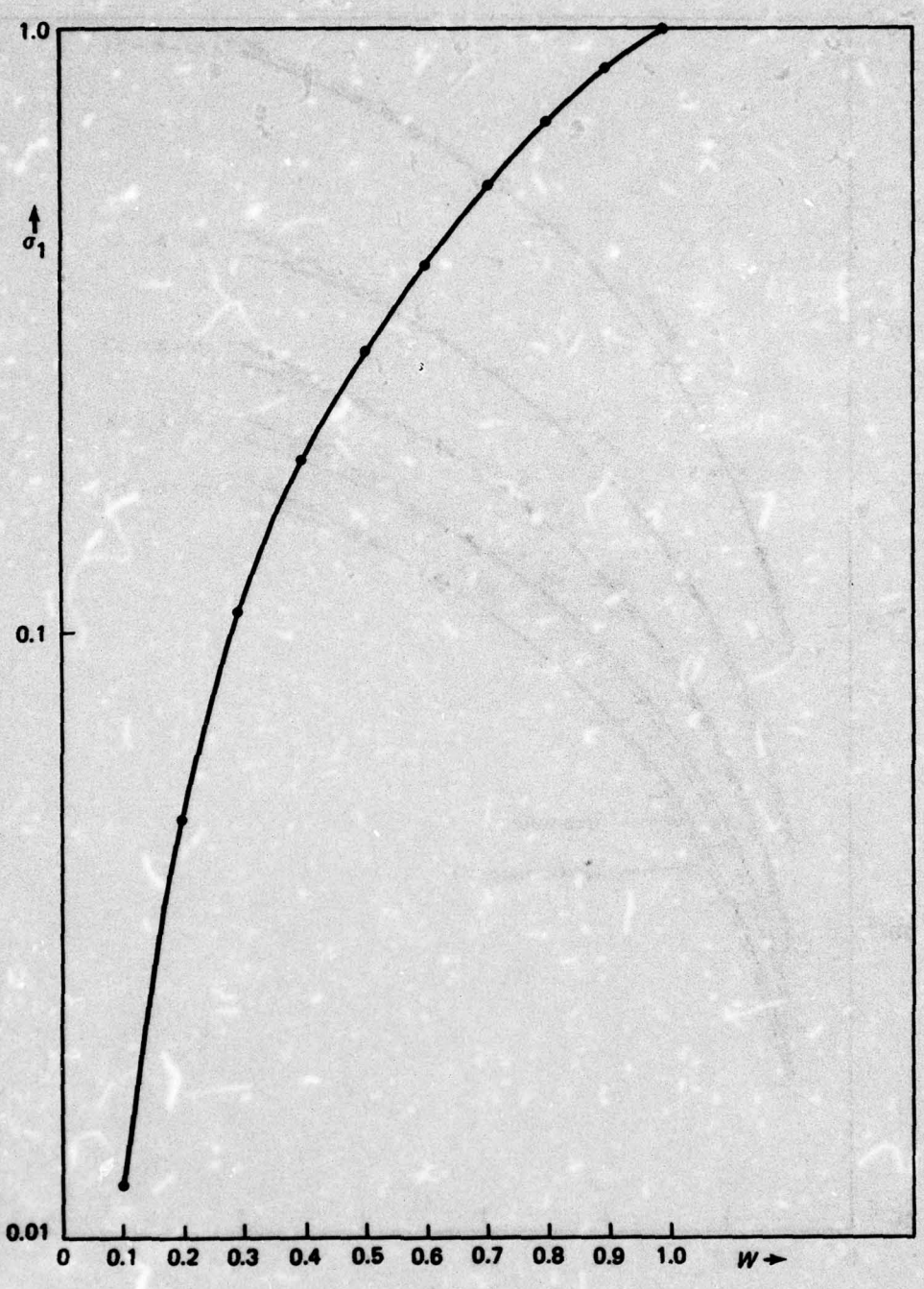

Figure 8. Plot of the normalized function σ_1; $\lambda\ \sigma_1(1) = 1$.

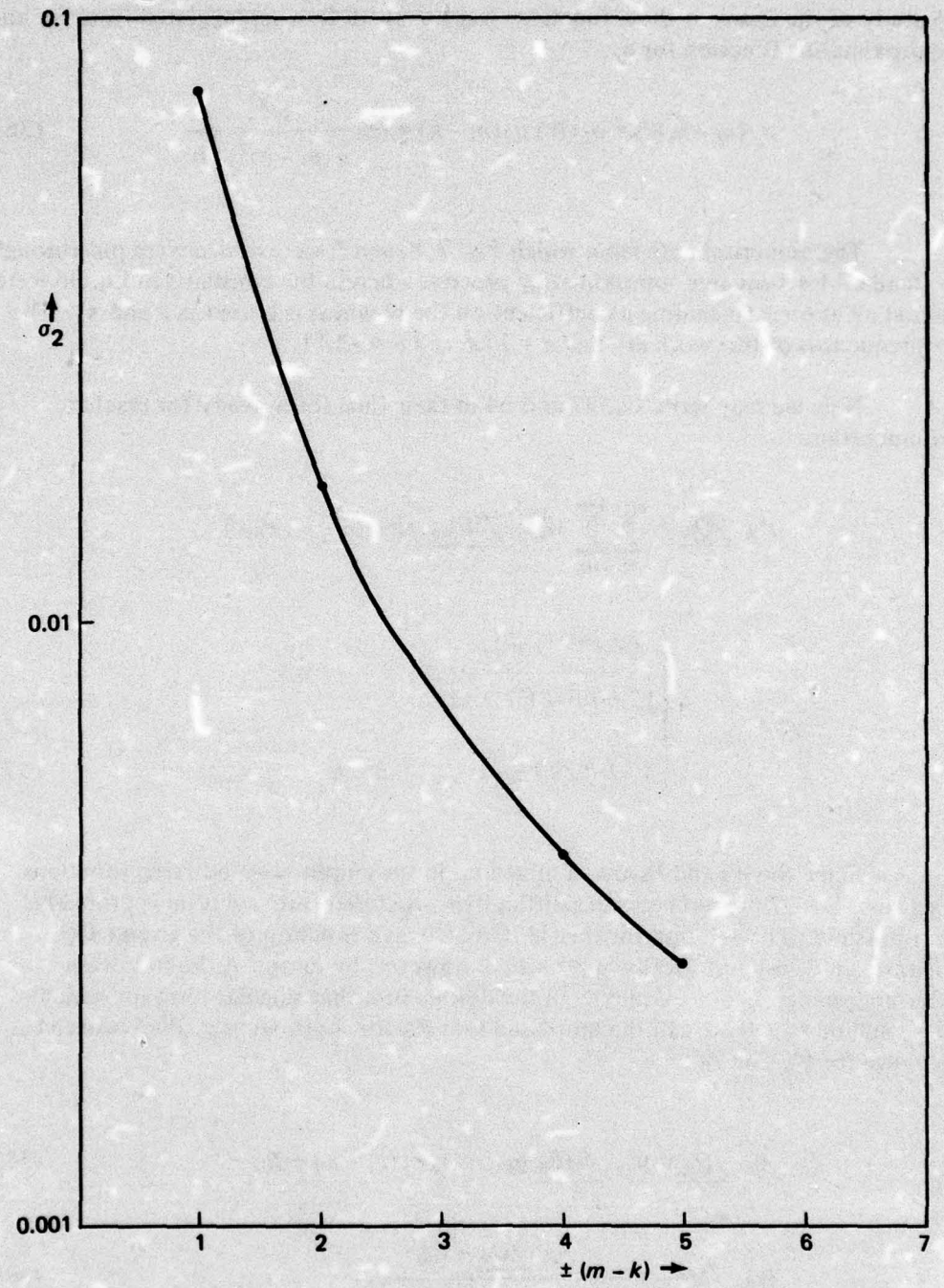

Figure 9. Plot of the denormalizing function σ_2.

A study of the forms of these functions leads to the following suggested form for an approximating function for σ_y:

$$\sigma_y\,(m-k,W) = \sigma_1(W)\,\sigma_2(m-k) = (\pm)\,\frac{W^2}{a\,(m-k)^2 + b} \tag{36}$$

The numerical data from which Fig. 7, 8, and 9 were drawn were put through a standard least-squares approximating process, wherein the constants in Eq. 36 were found all at once (including a coefficient on the W which is buried in a and b). The consequences of this work are that $a = 17.6$ and $b = -2.11$.

Now we may write Eq. 27 and 34 in their final form, ready for machine computation:

$$A_{jk}\,\angle\underline{Q_{jk}} = \sum_n \sum_m W_{nm}\,\angle\underline{MP_{nm}}\,\operatorname{sinc}\,(n-j+P_{nm})$$

$$\cdot \begin{cases} \dfrac{(-1)^{m+k+1}\,W_{nm}^2}{17.6(m-k)^2 - 2.11}\,; & m \neq k \\[2ex] 1 - 0.129\,W_{nk}^2\,; & m = k \end{cases} \tag{37}$$

Since the Ws and Ps are all mixed up in the amplitude-modifying functions (sigmas), Eq. 37 presents onerous difficulties. A closed-form solution is probably not possible. The solution for the (W,P) matrix as a function of the given (A,Q) matrix can be asymptotically approached, however, by means of the following rearrangement: Let us extract from the double sum that singular term for which $n = j$ and $m = k$. If we call the mutilated sum R_{jk} for short, we may then proceed to solve for W_{jk} and P_{jk}:

$$A_{jk}\,\angle\underline{Q_{jk}} = W_{jk}\,\angle\underline{MP_{jk}}\,\sigma_x(n=j)\,\sigma_y(m=k) + R_{jk} \tag{38}$$

$$W_{jk}\,\angle\underline{MP_{jk}} = \frac{A_{jk}\,\angle\underline{Q_{jk}} - R_{jk}}{\operatorname{sinc}\,(P_{jk})\,(1 - 0.129\,W_{jk}^2)} \tag{39}$$

For each (j,k) element in the matrix, A and Q are entered as W and P. Then R and the two sigmas are computed. These are fed back into the right-hand side of Eq. 39 to form a refined set of W and P. The process then may be repeated as many times as is deemed sufficient. Note that since both sigmas decrease rapidly as $|n-j|$ and $|m-k|$ increase, a great deal of computer time may be conserved during the computation for R if terms to be included in R are restricted to a disk centered on (j,k) and having a radius, say, of $|n-j|\,(m-k)^2 \leqslant 5$ or so.

Note that these disks must be handled properly when they extend beyond the edges of the matrix. Recall that the process of sampling a bounded function creates a sequence of "alias" replications of that function. The same is true in two dimensions. As a matter of fact, the optical analog is exact: Images formed from these holograms replicate across the image plane. Also, should the hologram itself be replicated checkerboard fashion, the image plane would not know the difference (except for a clever idea which will be covered below).

In view of these considerations, whenever a disk (for the computation of R) extends outside an edge of the matrix, one imagines that it is extending into a phantom replicated matrix; that is, matrix elements are appropriately taken from the corresponding opposite edge of the matrix.

Having established a rigorous derivation of a fundamental synthetic binary computer-generated hologram equation, we may proceed with a description of the process of setting up data for a hologram and producing that hologram.

PRODUCTION OF COMPUTER-GENERATED HOLOGRAMS

Procedures

Step 1: Choose an object size Δx. From this, compute the resolution element length in the hologram $\delta\nu = 1/\Delta x$.

Step 2: Determine the wavelength of light to be employed, λ, and the focal length of the lens, f. The cell size (Fig. 4) may then be found from $\lambda f \delta\nu = \lambda f/\Delta x$.

Step 3: The Fast Fourier Transforms available work most efficiently when the array size is a power of 2. Accordingly, select N to be 64 or 128 or the like. Then the actual hologram size will be N cell widths, or $N\lambda f\delta\nu$.

Step 4: The parameters c and M are design degrees-of-freedom. c is the constant width of the hole, and clearly the smaller that c is, the better the phase determination at each hole will be; but of course the image will become dimmer. Thus, c

is the brightness-quality trade-off parameter. As discussed above, M will determine in which diffraction order the primary image will appear, and will also dictate the source offset. Equation 19 assigned M as an integer, but this was for analytic tidiness. There is a case to be made for noninteger M, to be covered below. It is important to realize that c and M are not quite independent, as argued in the next step.

Step 5: Prepare the data. Numerically describe u_{nm}. In accordance with Eq. 20, $c\ (n/N + M)$ is the argument of the sinc function by which the data array u_{nm} is to be divided in order to create v_{nm}. Since in fact index n is an artifice ranging from 1 to N (negative indices are not allowed in Fortran DO Loops), it must appear in the conversion process from u to v in the following way. From Eq. 18:

$$v_{nm} = \frac{u_{nm}}{\text{sinc}\left[c\left(\frac{n - N/2}{N} + M\right)\right]} \tag{40}$$

It is important to notice that when $n = N/2$, the product cM dominates. cM must not be allowed to become an integer, or spurious delta functions will be introduced into the data for v. Aiming for an image in the first diffraction order, we may set $M = 1$ and choose $c = 1/2$. Similar choices for c must be carefully made for other Ms.

Step 6: In accordance with Eq. 23, allow the factor $c\,(\delta\nu)^2$ to be absorbed into the proportionality constant K, and perform a two-dimensional Fast Fourier Transform on array v to produce array V, which is now identified as the complex array

$$A_{jk} \angle Q_{jk}$$

Step 7: Present the complex (A,Q) array to Eq. 39 and the iteration description following it. Iterate to a solution.

Step 8: Plot, photographically reduce, and use.

Strategic Improvements

Although the process of production described above will yield usable holograms, there are several strategems which can be invoked to greatly enhance the quality of the formed image. There are also a few subtle flaws in the derivation which only come to light after some production experience.

1. First there is the matter of knowing when to stop the iteration. Equation 39 does not lend itself readily to an analysis of convergence criteria. Indeed, there is an implicit assumption in the derivation that the process will converge. But this is not necessarily true. Under certain pathological conditions of the input data field, some cells in the matrix may have no solution, while others may have more than one. Should this occur, the iteration will be perturbed by "bad spots" in the matrix and oscillate rather than converge. By the nature of the "R disk" described earlier, such bad spots will adversely influence their neighboring elements. A way around this difficulty will be presented later in this report. Other than that, the matter of terminating the iteration is perhaps best handled empirically. Experience has shown that five times around the loop of Eq. 39 is usually sufficient.

2. One trick which greatly improves image brightness without sacrificing image quality is the introduction of random phase into the initial description of the u_{nm} field. This "smears out" the larger holes, which otherwise tend to clump in the center of the hologram, leaving most of the hologram plane essentially opaque.

3. Associated with the idea of introducing random phase is the notion of producing replicated holograms of the same object field (checkerboard fashion), but introducing uncorrelated random phase in each replication. Thus, the image, which is correlated across the replications, will be enhanced, while the background noise will tend to cancel out.

4. It was mentioned earlier that M was analytically constrained to be an integer. This results in images formed near the zero-order bright spot in the image plane, with other image orders located close to corresponding other-order bright spots. These regions are particularly noisy in the image plane, and it is to one's advantage to locate the formed image between them. This implies that M should be an odd number of 1/2 integers. A value of 3/2 for M works as good as any and places the image nicely in the quietest part of the image plane (Ref. 7).

5. Closely allied with the choice of M is the choice of c. With a naive choice of M and c, a phenomenon is prone to occur which has acquired in the literature the name of the "gap and overlap problem." What happens is that the hole may extend outside of its cell and possibly overlap with the adjacent hole where, strictly speaking, the hologram should have a transmittance of 2. These events also leave unsightly gaps between holes.

A little bit of algebra applied to Fig. 4 shows that with $M = 3/2$, the hole will be displaced only to the edge of the cell when c has a value of 1/3. This nicely banishes the gap and overlap problem, and also improves image quality, since the hole is

smaller than when $c = 1/2$. Since $|MP| \leq 1/2$, $|P| \leq 1/3$ when $M = 3/2$. That is, the hologram should now be illuminated at an angle somewhat steeper than that which would produce a 2π phase change across the cell.

At the same time, the input data field has to be "tricked" into "thinking" that the image is in the 3/2 diffraction order. This is most easily done by "rotating" the numerical data in the u_{nm} field sideways. That is, the left- and right-hand halves of the data field are initially simply interchanged (or the data can simply be set up in this way) before the Fast Fourier Transform process which produces V is invoked.

6. Another trick to enhance image brightness is to scale the data array for the amplitudes prior to plotting by, say, a factor of 1.5, and then to "clip" the amplitude data to unity. At the same time, a great deal of plotter time can be eliminated by simply deleting from the plotting list those holes for which the amplitude is below a certain minimum. A convenient minimum point may be determined from the width of the pen line. There is no point in attempting to plot such holes, and one might as well conserve on plot computations.

7. It is beneficial to plot with black ink on vellum paper.

8. During the photographic reduction process, it is advisable to overexpose and underdevelop to enhance contrast in the hologram.

THE POLYNOMIAL FIT METHOD

Reference 8 is the source of the basic idea explored here. It is important to realize that because of the cyclic nature of P and Q, we may actually write, in the zeroth approximation from Eq. 39 when $R = 0$ and the sigmas are unity:

$$MP_{jk} = Q_{jk} + L_{jk} \tag{41}$$

where L is any integer.

This somewhat subtle point, which was overlooked in the prior derivation, will play an important part in this section of the report.

It is now time to take a very careful look at what the phase relationship on the hologram plane looks like under conditions of tilted plane wave illumination and, for simplicity, $M = 1$. Recall that the plane of the hologram is partitioned into cells $\lambda f \delta\nu$ on a side, where λ is the illumination wavelength, f is the focal length, and $\delta\nu = 1/\Delta x$ is the resolution element, Δx being the image size. One such resolution cell, containing its hole, is shown in Fig. 10.

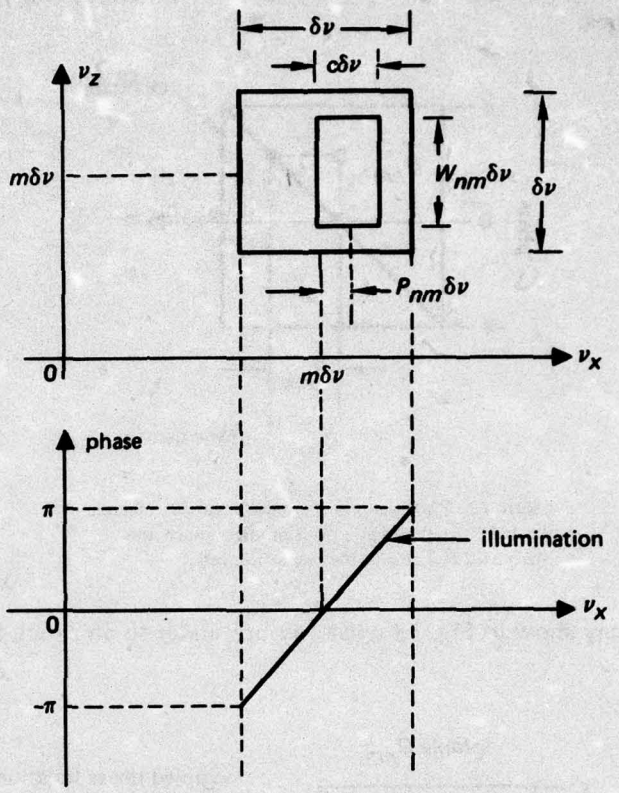

Figure 10. Resolution cell and its associated illumination function, shown for the case $M = 1$.

Now we can present Fig. 11, which shows the succession of phase in a string of cells in the n direction (fixed m).

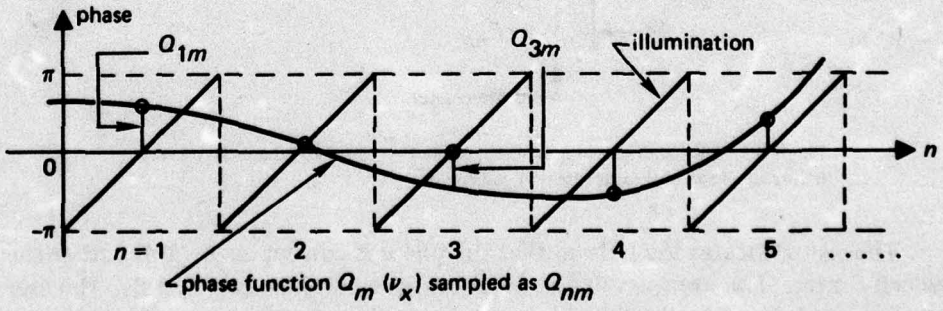

Figure 11. Succession of phase samples in a string of resolution cells.

We are now in a position to show in Fig. 12 exactly what the zeroth approximation does.

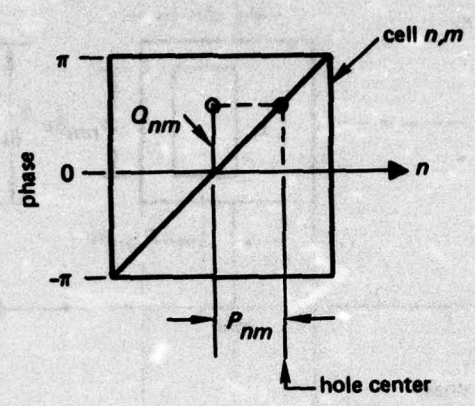

Figure 12. The zeroth order approximation, wherein the hole is centered at a position dictated by the phase at the center of the resolution cell.

And we may show in Fig. 13 what any pretender to an exact solution should accomplish.

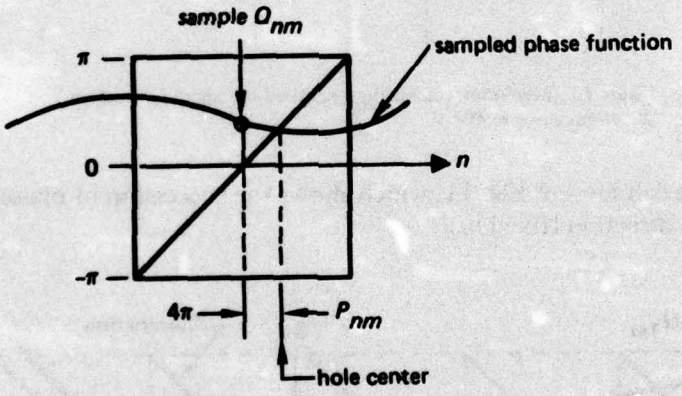

Figure 13. The exact solution, wherein the hole is centered where the phase is correct at the hole rather than at cell center.

That is: P locates the hole so that the phase is correct *at the hole* rather than at the cell center. The iteration of Eq. 39 attempts to do just exactly this. Having properly located the hole, the set of W can be directly calculated from P and a knowledge of the A_{nm} function, again *at the hole.*

An obvious drawback to this is that a knowledge of the Fast Fourier Transform at the sampling points (cell centers) is no longer enough. However, rather than increase the "fineness" of the sampling which, to be at all effective, would expand the size of the Fast Fourier Transform unreasonably, one may use the Q_{nm} data to establish piece-wise polynomial fits over a few cells embracing the cell in question.

What happens when a phase function $Q_m(n)$ (it is written explicitly that way to emphasize the Q as a function of n, there being a set of such functions indexed by m) bobbles around π? The smooth curve in Fig. 11 becomes a sequence of disjointed "up and down" points from cell to cell. In such a case (which is certainly to be expected from time to time) any attempt at interpolating will lead to disaster. But since, according to Eq. 41, we are free to modify P by any integer L, let us replace Fig. 11 by Fig. 14.

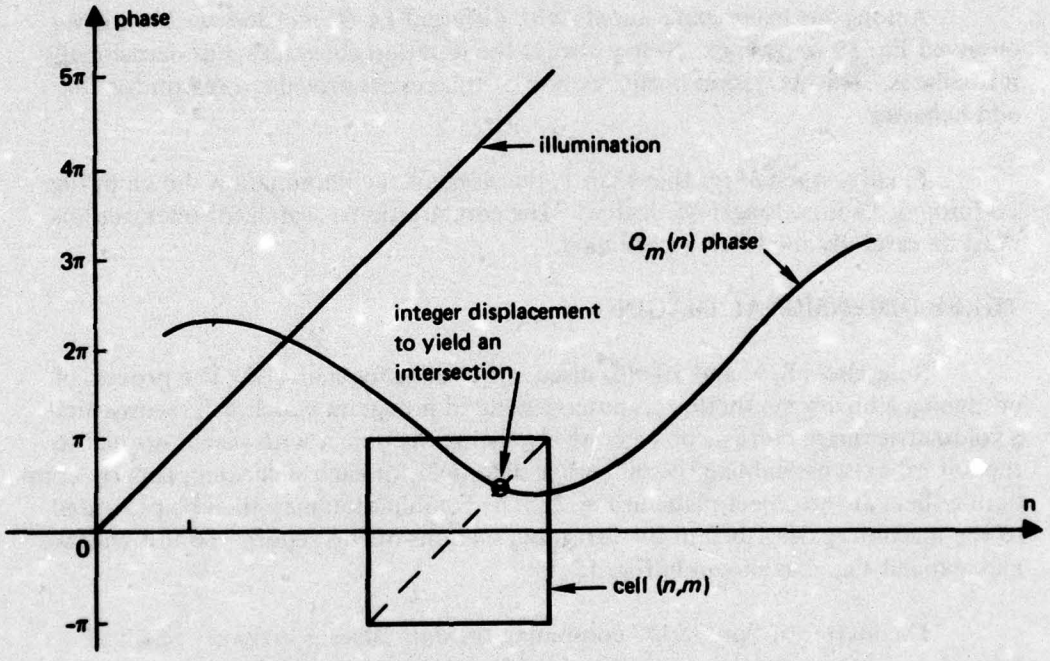

Figure 14. Schematic illustration of a method of solution which recognizes that the illumination phase is modulo 2π.

To recapitulate: The desired (A,Q) matrix having been established, we produce (for each m in turn) an interpolating polynomial embracing the (n,m) cell in question (in the n direction), heeding the need to effect a translation of the matrix during close-to-edge conditions. We then add or subtract whatever integer L it takes to get an intersection between the illuminating phase function and the function Q.

The horizontal distance from that intersection to the center of the cell is the exact solution for P for that cell, giving the correct phase transmittance for the hologram *at the hole*. P is then entered into the corresponding amplitude function $A_m(n)$ (suitably interpolated itself) for an exact solution for W.

Although the function $Q_m(n)$ is known to be single valued in the parameter n, it still may happen that Q intersects the illumination phase function more than once in a cell. Any of these solutions are equally valid, and one might be advised to simply pick that one which is nearest to the cell center.

Then, too, it may happen that a certain cell has *no* such intersection for *any* L (see cell 5 in Fig. 11). This cell should then be skipped entirely when the plot file is being assembled.

Among our many experiments with different (A,Q) matrices we have never observed Eq. 39 to diverge. Nearly always the iteration converges, but occasionally it oscillates. The discussion in this section of this report provides a reason for this odd behavior.

Finally, when M is other than 1, the slope of the illumination shown in Fig. 10 through 14 is no longer 45 degrees. The computational search for intersections must be carefully modified accordingly.

THREE-DIMENSIONAL IMAGING

References 8, 9, and 10 also discuss the following material. The process of producing a binary synthetic computer-generated hologram which will reconstruct a volumetric image consists of successively slicing the object with planes normal to the optical axis; assembling the numerical data field for each slice; and properly combining them at the object plane in Fig. 2. The combination may then be presented to the machinery described in the foregoing sections of this report. To this end, we may expand Fig. 2 as shown in Fig. 15.

The matter of "properly" combining the data slices is variously resolved depending on the optical relationships between the contents of the slices. Object content slice-to-slice may be noninterfering (mutually offset), or the slices may mutually scatter in a translucent, or in an opaque manner.

To reconstruct an image at a position displaced on the optical axis by an amount corresponding to its displacement in the original object space, perhaps the most straightforward method is to take advantage of the following observations.

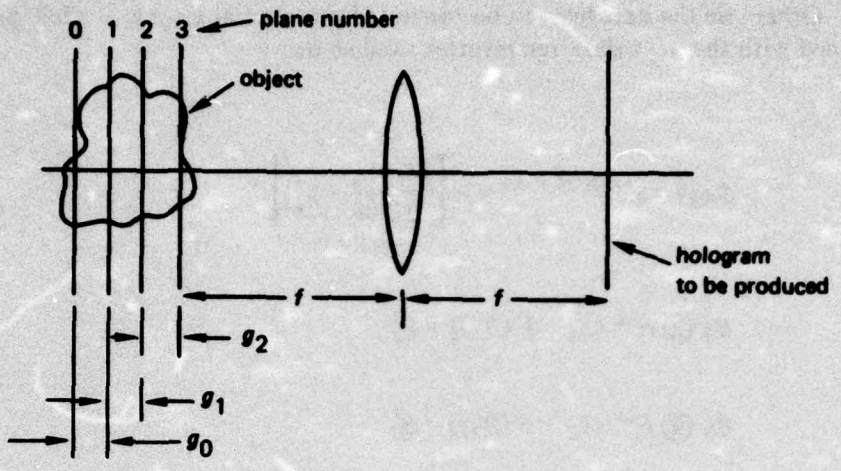

Figure 15. Optical setup to be synthesized on the computer for producing a hologram of a volumetric object.

To describe the wavefront from plane 0 (Fig. 15) with coordinates (x_0, y_0) as it impinges upon plane 1 with coordinates (x_1, y_1), one may make use of the Fresnel approximation:

$$a(x_1, y_1) = \iint b(x_0, y_0)\, E\left\{-\frac{1}{2\lambda g_0}\left[(x_0 - x_1)^2 + (y_0 - y_1)^2\right]\right\} dx_0\, dy_0 \tag{42}$$

From the convolution theorem, Eq. 1, this may be stated as:

$$A(\nu_x, \nu_y) = B(\nu_x, \nu_y)\, E\left[\frac{\lambda g_0}{2}(\nu_x^2 + \nu_y^2)\right] \tag{43}$$

The exponential factor in Eq. 43 serves as a "shifter" down the optical axis. After the object is sliced as finely as circumstances dictate, Eq. 43 is used to prepare the data for combining. The process may possibly be done all at once at the front focal plane (ready for conversion to holographic plotting data) if the object slices are nonoverlapping:

$$A(\nu_x, \nu_y) = \sum_i B_i(\nu_x, \nu_y)\, E\left[\frac{\lambda g_i}{2}(\nu_x^2 + \nu_y^2)\right] \tag{44}$$

Otherwise the data have to be converted one slice at a time, shifted, properly combined with the next slice, reconverted, and so on:

Let

$$S_i(g) = e^{i\pi\lambda g_i(\nu_x^2 + \nu_y^2)} = E\left[\frac{\lambda g_i}{2}(\nu_x^2 + \nu_y^2)\right] \tag{45}$$

then

$$B_2 \circledast F^{-1}\,(S_1 \cdot F(B_1)) = B_2'$$

$$B_3 \circledast F^{-1}\,(S_2 \cdot F(B_2')) = B_3'$$

$$\vdots$$

$$A(\nu_x, \nu_y) = B_i \circledast F^{-1}\,(S_{i-1} \cdot F(B_{i-1}')) \tag{46}$$

where the symbol $\circledast$ indicates complex multiplication in the case of translucent interference, and bodily replacement of data in the case of opaque interference.

RESULTS

Some representative results of our work are presented in the following plates.

Figure 16 is a reproduction of part of a hologram. (They all look more-or-less alike to the eye.)

Figure 17 is a reproduction of the image "NUC" in the first diffraction order. Note that the zero-order noisy background interferes considerably with image clarity.

Figure 18 shows an object which consists of a bright square in back of an opaque cross. The reconstruction has been moved to the 3/2 order, where background interference is minimal.

Figures 19, 20, and 21 were all taken from the image field of *one* hologram. The camera was simply focused at different planes along the optical axis. This set of plates illustrates a true three-dimensional (real) image reconstruction. Here, the adjoining noisy background in each case is simply the out-of-focus other two letter objects of the field.

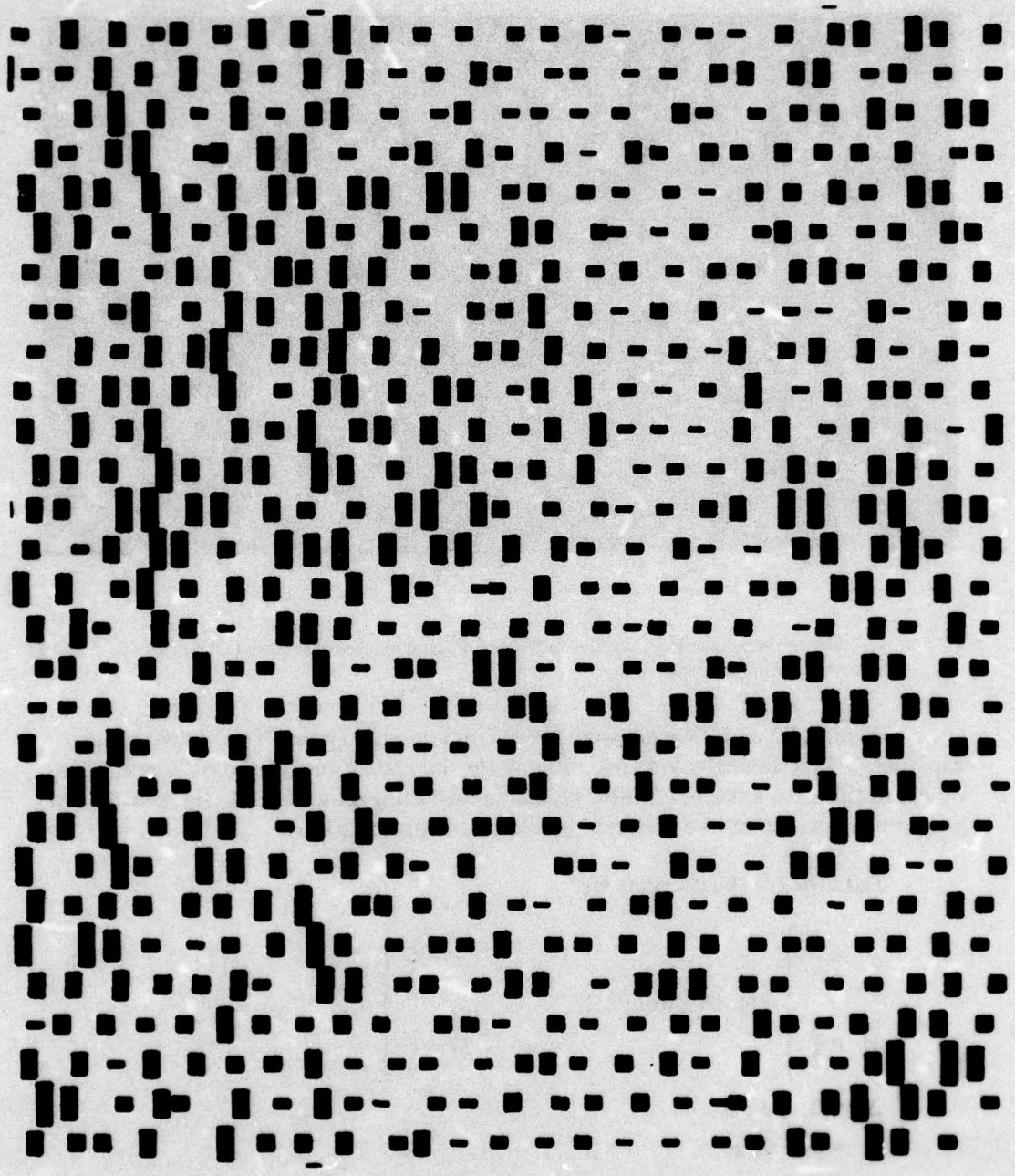

Figure 16. Portion of a computer-generated synthetic binary hologram plot. The entire plot is a square 15.36 inches on a side. Each resolution cell in this plot is 0.24 inch on a side. $c = 1/3; M = 3/2$. The plot is to be reduced by a factor of 500. The plot is actually a "negative" in that the dark rectangles become the transparent holes in the hologram.

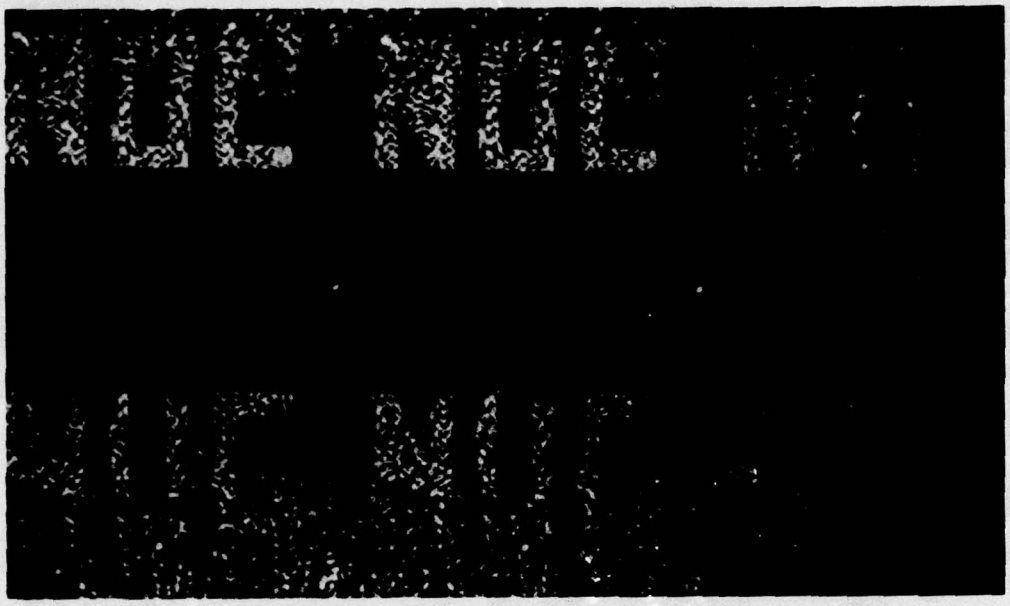

Figure 17. Reproduction in the first diffraction order. The zero-order noisy background interferes with the image.

Figures 22 and 23 again were taken from *one* hologram. They illustrate the capability of producing volumetric imaging for the case of opaque interference. The object in this case was a bright disk behind an occulting dark disk. Again, the camera was simply focused at two different places on the optical axis.

Data for the illustrations are:

$c = \frac{1}{3}$, $M = \frac{3}{2}$ } Fig. 18 through 23

$c = \frac{1}{2}$, $M = 1$ } Fig. 17

$\Delta x = 0.422$ cm

$\lambda = 0.5145\ \mu$

$f = 10$ cm

$N = 64$

Photographic reduction factor = 500

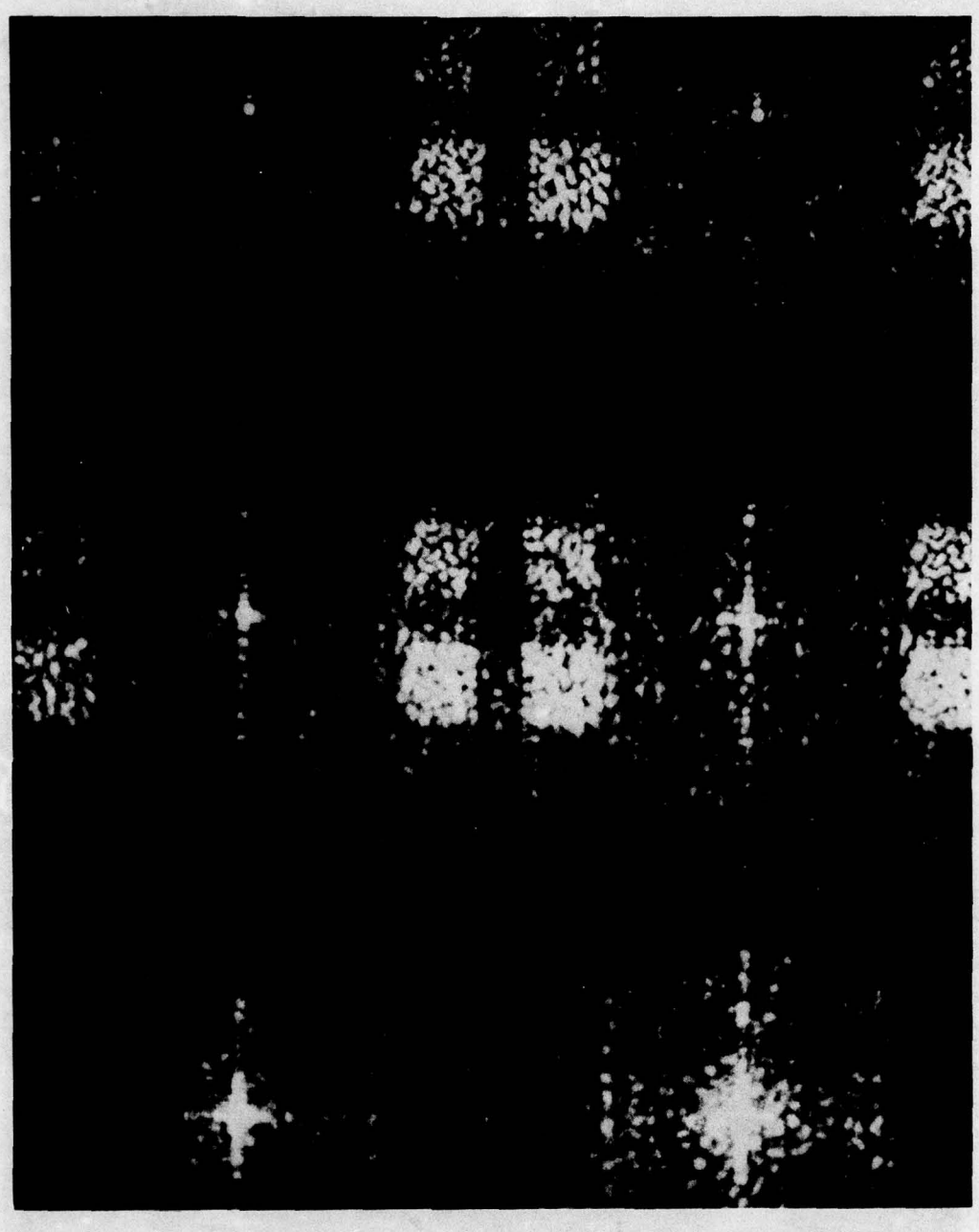

Figure 18. Reconstruction in the 3/2 diffraction order, where the background noise is minimal.

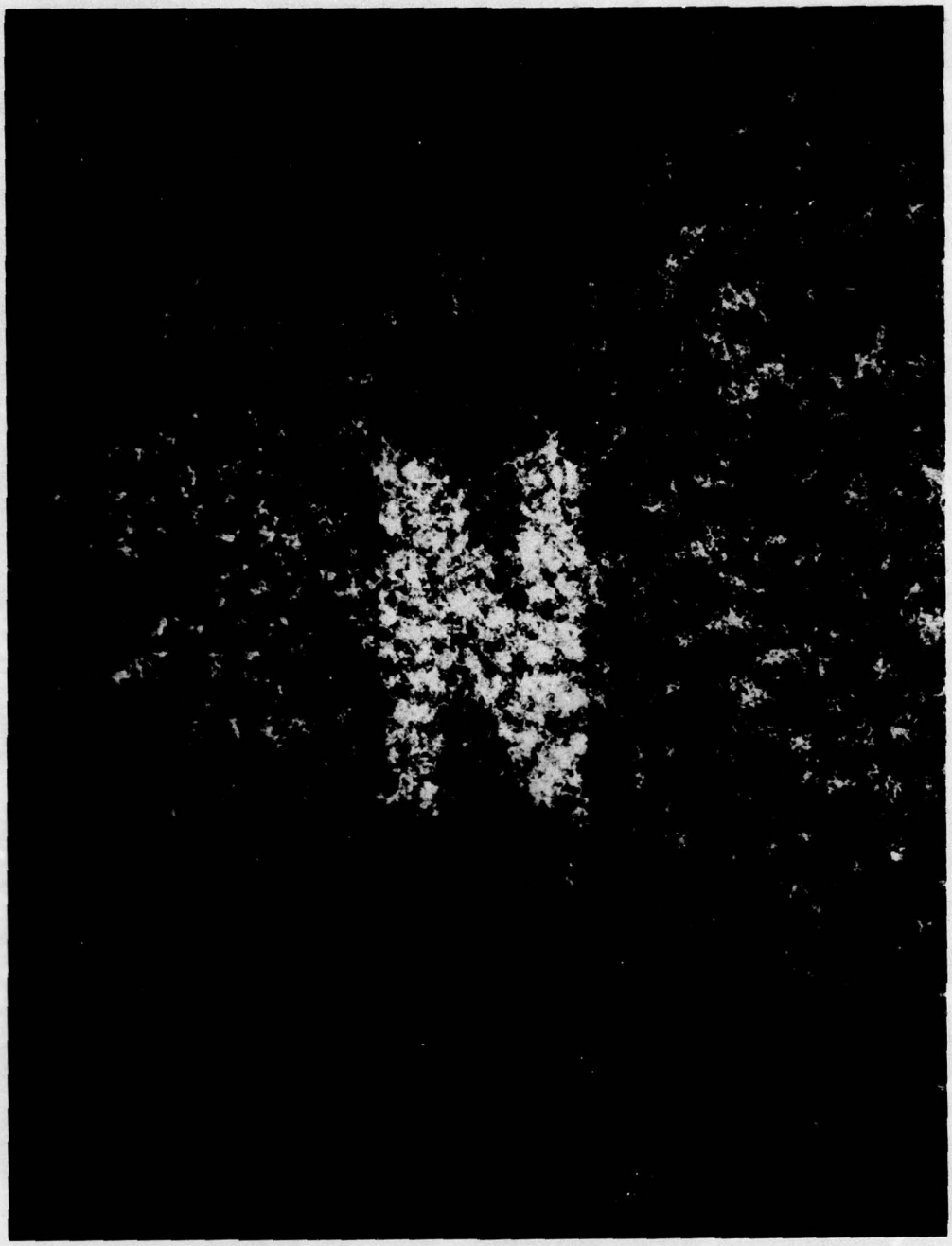

Figure 19. First of three images formed by one hologram. This illustration, along with Fig. 20 and 21, illustrates volumetric imaging in the case of a non-self-interfering object.

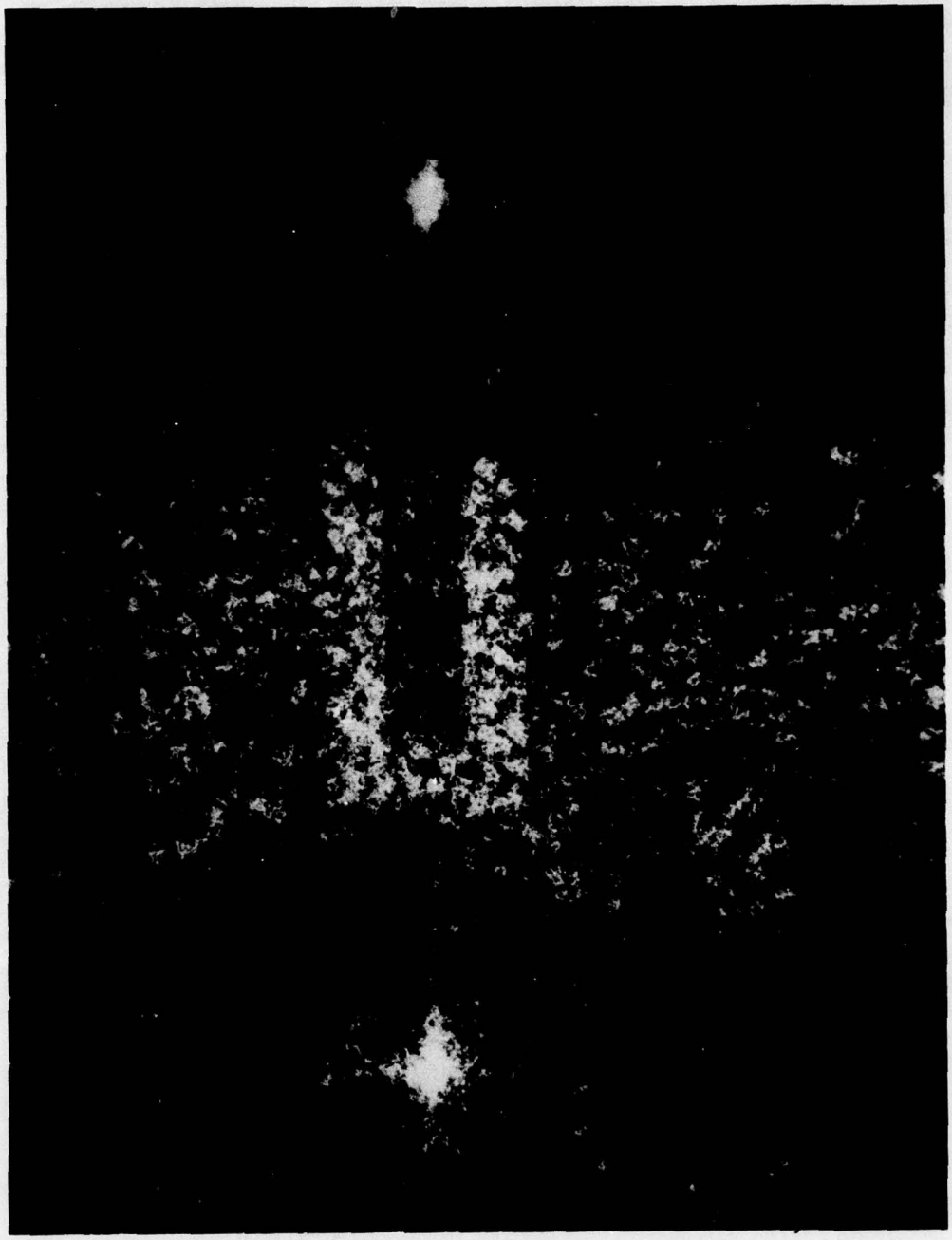

Figure 20. Second of three images taken from one hologram.

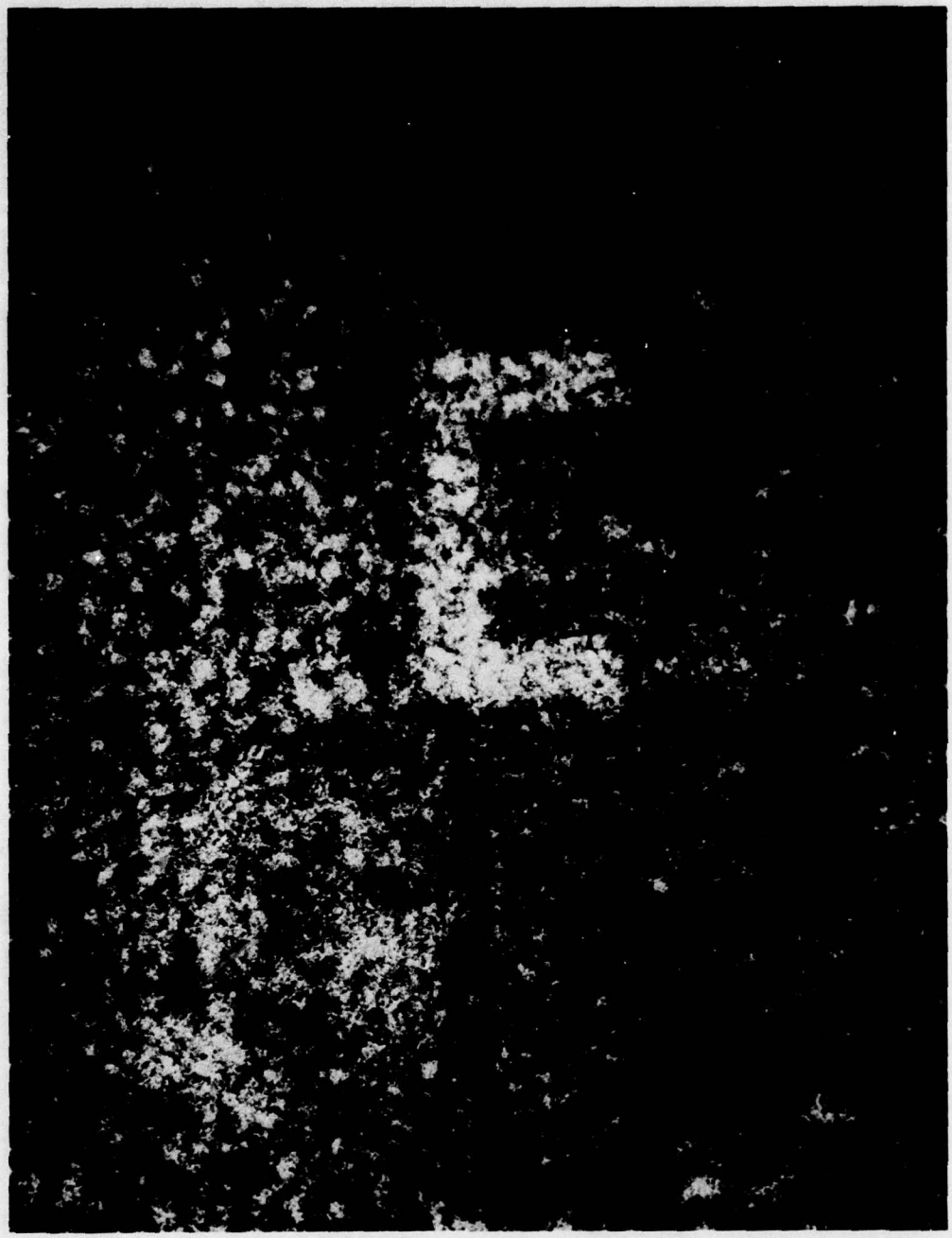

Figure 21. Third of three images taken from one hologram. The images of Fig. 19, 20, and 21 were mutually separated along the optical axis by 2 cm.

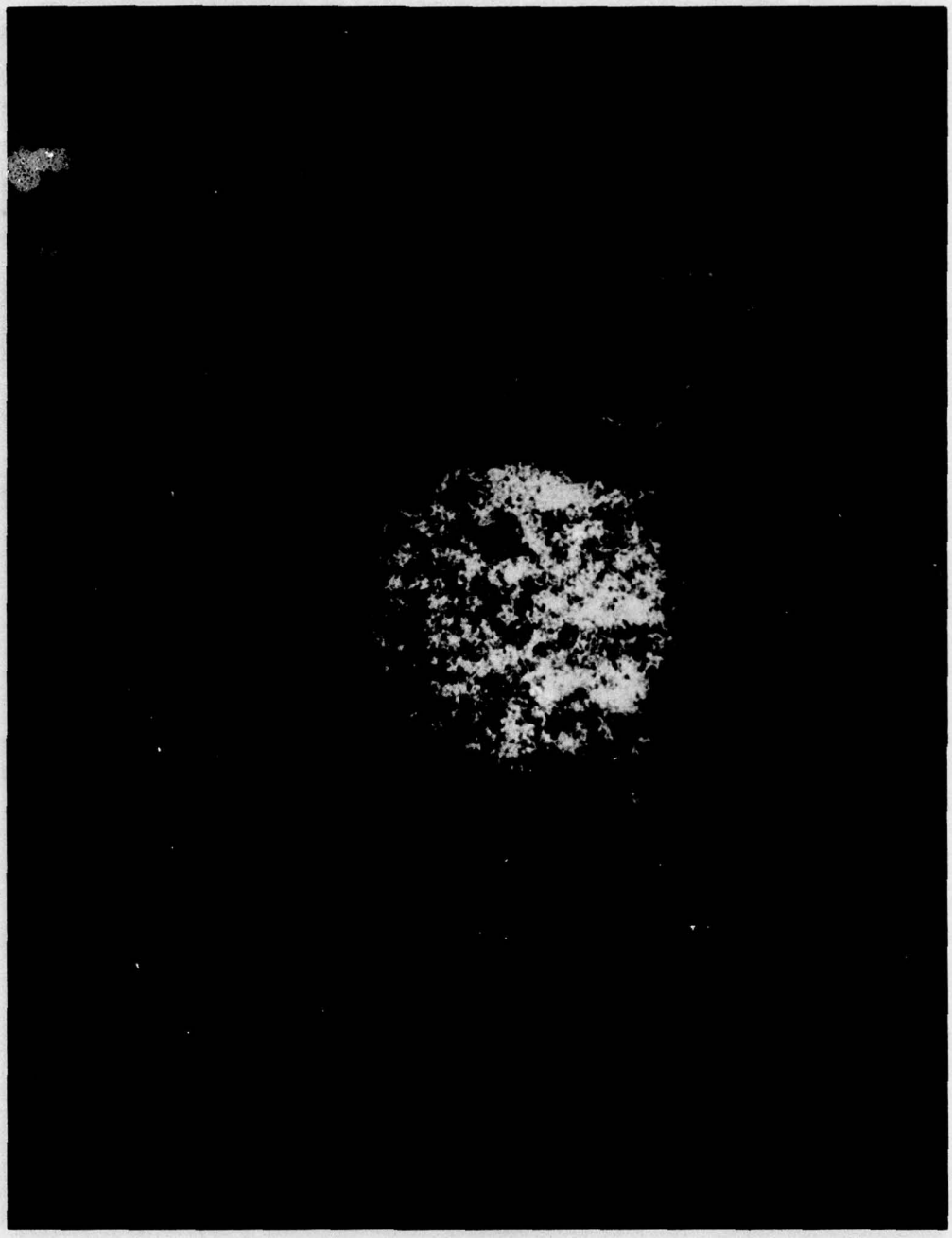

Figure 22. This halftone, together with Fig. 23, illustrates volumetric imaging in the case of a self-interfering object.

Figure 23. Second of two images taken from one hologram. This image was 1 cm down the optical axis from that of Fig. 22 and illustrates the capability of volumetric imaging of an object which self-interferes (self-occults).

It is of note that the "polynomial fit" method requires less computer time than does the "iteration" method by a factor of about 1/5 for a 64 X 64 data field.

FUTURE WORK

The next step to speed up the process of producing binary synthetic computer-generated holograms is to circumvent the Cal Comp plotting operation and have the computer plot the hologram directly on the face of a cathode ray tube (CRT). The photographic reduction could then be done directly from the CRT. Since it is relatively difficult to write programs which vary the size as well as the position of a spot on a CRT face, alternatives to Fig. 4 may have to be investigated.

One attractive alternative (doubtless there are many others depending on the ingenuity of the investigator) is given in Ref. 11 and is illustrated in Fig. 24. Here, the cell contains *two* holes which always maintain the same size. Phase encoding is accomplished, as before, by the position of their "center of gravity" in the x direction, but now the amplitude is controlled by an entirely different mechanism. The amplitude is controlled, roughly speaking, by diffracting light which is unwanted to orders other than that in which the primary image is being formed. This may be seen from Eq. 47:

$$AE(Q) = A_1 E\left[P_{nm} + \frac{d}{2}\right] + A_1 E\left[P_{nm} - \frac{d}{2}\right]$$

$$= 2A_1 \cos(\pi d) E(P_{nm}) \qquad (47)$$

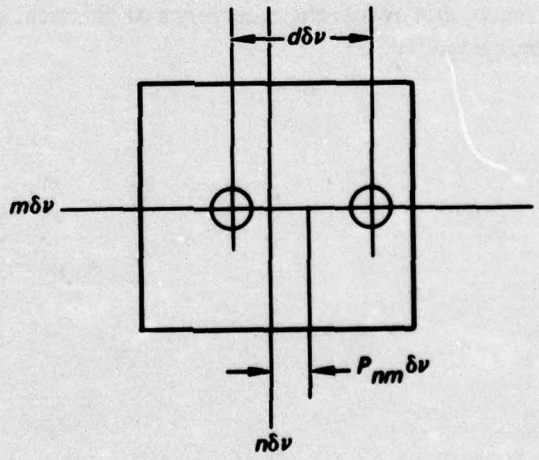

Figure 24. Resolution cell containing two-hole method of encoding phase and amplitude.

where A_1 is the amplitude of an individual hole. It can be seen that the resulting amplitude depends directly on the spacing, d, and in particular that the amplitude is zero when $d = 1/2$.

This process can be expected to suffer many of the same fine points as the iteration method, Eq. 39, experiences. In particular, the gap-and-overlap problem discussed earlier is with us again here. However, the holes may be aligned vertically, thus diffracting unwanted light in the y direction. A quick analysis similar to Eq. 47 will show that the resulting amplitude control by hole spacing is still valid.

These and other avenues of hologram construction are to be explored. Eventually it is hoped that these techniques can be brought directly to bear on the spatial light modulator devices referred to in the Introduction.

CONCLUSIONS

In-house expertise at NUC can now be said to have reached the point where data for the construction of a hologram which will produce volumetric imaging can be produced at will for an arbitrary object.

The work thus far has employed Cal Comp plots followed by photographic reduction because of convenience, and because the "how-to" aspects of this effort have been more important than speed of hologram formation at this time. Image quality has been steadily improved, and at the same time production costs have been reduced, by means of careful refinement of computer programs.

The process of optical real-time signal processing via computer-generated holograms is within reach, and awaits the emergence of practical spatial light modulator devices to become a reality.

REFERENCES

1. Binary Fraunhofer holograms generated by computer. Lohmann and Paris; Applied Optics, Vol. 6, No. 10, Oct 67. P. 1739.

2. A thermoplastic input data modulator for real time optical processing of data. Cindrich, Currie, and Leonard; Environmental Research Institute of Michigan, Ann Arbor.

3. Applications of coherent light valve systems to optical signal processing. Noble and Penn; General Electric Company, Electronics Laboratory, Syracuse.

4. Real time optical processing. Nisenson, Feinleib, and Iwasa; Itek Corp., Central Research Laboratories, Lexington, Mass.

5. Reusable optical image storage and processing device. Feinleib and Oliver; Applied Optics, Vol. 11, No. 12, Dec 72. P. 2752.

6. A new real-time non-coherent to coherent light image converter: the hybrid field effect liquid crystal light valve. Grinberg et al.; Hughes Research Laboratories, Malibu; NASA Contract NAS5-23192.

7. Improving binary computer holograms. Becker and Dallas, Optics Communications, Vol. 15, No. 1, Sept 75. P. 50.

8. Computer generated binary holograms. Brown and Lohmann; IBM J. Res. Develop., March 69. P. 160.

9. Scanning halftone plotter and computer generated continuous tone holograms. Ichioka, Izumi, and Suzuki; Applied Optics, Vol. 10, No. 2, Feb 71. P. 403.

10. Introduction to Fourier optics. Goodman. McGraw-Hill Book Company, San Francisco, 1968. P. 60.

11. New coding technique for computer generated holograms. Haskell and Culver; Applied Optics, Vol. 11, No. 11, Nov 72. P. 2712.

INITIAL DISTRIBUTION

Naval Air Systems Command (NAIR-604)
Naval Sea Systems Command
  SEA-060
  SEA-09G3
  SEA-09G32 (4)
Naval Air Development Center
Civil Engineering Laboratory
Naval Coastal Systems Laboratory, Panama City
Naval Electronics Laboratory Center
Naval Missile Center
Naval Surface Weapons Center, White Oak
Naval Postgraduate School (Library, Technical Reports Section)
Naval Research Laboratory
Naval Ship Research and Development Center, Annapolis Division
David W. Taylor Naval Ship Research & Development Center, Bethesda
Naval Underwater Systems Center, New London Laboratory
Naval Underwater Systems Center, Newport Laboratory
Naval Weapons Center (Code 753)
Chief of Naval Operations (Systems Analysis Division) (NOP-966)
AFSPCOMMCEN/SUR, San Antonio, TX 78243
UK Scientific Mission, British Embassy (UNCL/A ONLY)
Dr. Wm. Dallas, Virginia Polytechnic Inst. & State Univ.
Defense Documentation Center (12)

Center Distribution:

00	45
01	4521
02	30
03	301
05	65
11	6501
14	6511
15	6513
25	6562 (25)
301	6565 (2)
3014 (5)	6566 (1)
35	90
40	96